A Variable Structure Approach for Finite-Control-Set Model Predictive Current Control of a Household Appliance

Eleonora Brasili [1], Luigi Fagnano [2], Gianluca Ippoliti [3], Giuseppe Orlando [4]

***Abstract*— A finite control set model predictive control (FCS-MPC) strategy is investigated for the speed regulation of permanent magnet synchronous motors (PMSMs). A cascaded control structure is implemented, consisting of an inner FCS-MPC current loop, enhanced by a variable structure (VS) approach, and an outer discrete-time VS control (DTVSC) speed loop. The adoption of FCS-MPC for current regulation in industrial PMSMs is driven by its inherent fast dynamic response, ability to enforce constraints, and the potential for modulator-less operation. Furthermore, DTVSC has proven to be an effective PMSM control strategy, particularly valued for its robustness in the face of model inaccuracies and external disturbances. The proposed control methodology, compared to the industry-standard PI cascaded control implemented by Whirlpool in domestic appliances, provides an improvement in control performance and robustness characteristics.**

I. INTRODUCTION

Electrical drives are fundamental for electromechanical energy conversion, powering a wide range of devices from household appliances to critical industrial systems. The evolution of electronically switched semiconductor devices within power electronic systems has resulted in the widespread adoption of three-phase AC motor drives, replacing DC machines due to the enhanced structural reliability offered by AC motor technology. More specifically, the 2-Level Voltage Source Inverter (VSI) driving a Permanent Magnet Synchronous Motor (PMSM) represents the dominant configuration within servo drive systems [1] [2].

Field Oriented Control (FOC), based on the space vector concept, is a conventional control architecture for PMSMs [1]. This method involves transforming three-phase quantities into a rotating $d-q$ reference frame, where proportional-integral (PI) controllers regulate the signals, and Pulse Width Modulation (PWM) generates the required three-phase voltages [3].

Directly controlling semiconductor switches provides the most effective and practical means of managing power converters and machine drives, but the operational constraints of electronically switched semiconductors are critical aspects in control system design and implementation [4] [2]. In this operational environment, Model Predictive Control (MPC) has demonstrated a robust capacity for optimal constraint enforcement [5] [6].

[2]Luigi Fagnano is with *Whirlpool Technology Service S.r.l.* 60044 Fabriano (AN), Italy luigi_fagnano@whirlpool.com

[1]Eleonora Brasili, [3]Gianluca Ippoliti and [4]Giuseppe Orlando are with *Dipartimento di Ingegneria dell'Informazione* Università Politecnica delle Marche 60131 Ancona, Italy e.brasili@pm.univpm.it, gianluca.ippoliti@univpm.it, giuseppe.orlando@univpm.it.

In contrast to conventional MPC strategies that employ PWM for semiconductor switch gate signal generation, the methodology investigated in this paper provides a simplified control system realization. The gate signal is determined by directly minimizing the error between the desired control signals and those which can be realized by the semiconductor switches [3] [7]. The designation FCS-MPC, as seen in literature such as [8] [5], refers to this minimization technique that utilizes a cost function. Reference [6] provides an analysis and comparison of various FCS-MPC schemes and their performance. Key attributes of FCS-MPC are its quick dynamic response, constraint enforcement, and potential modulator elimination. Due to these advantages, it has become a central area of research in MPC for power electronic systems [9]–[11].

To ensure robust closed-loop performance against electromechanical parameter variations, this paper adopts a Variable Structure Control (VSC) approach [12]–[15] for FCS-MPC. Additionally, since FCS predictive control is primarily used for current regulation, a VS velocity control is also designed for PMSMs. VSC methods are recognized for their significant robustness and invariance to matched uncertainties [13], and offer computational simplicity compared to other robust control techniques like adaptive, H_∞, integrator backstepping, and neural network-based control [16]–[20].

In this paper, to adequately address the challenges of sampled-data systems, such as robustness, which is crucial for practical discrete-time implementation on a DSP in a real motor drive, a solution based on DTVSC [21] [22] is proposed. In particular, the solution adopted implements FCS-MPC for inner current control, where the optimal values of the control variables are assigned by a DTVSC law, and a pure DTVSC for outer velocity control, thereby extending the typical PI cascade control structure for PMSMs [12] [13] (see Fig. 1). Moreover, to evaluate the proposed control law, the highly accurate Whirlpool simulation program, designed for household appliances, was employed. A comparison of the proposed architecture with the standard PI control used by Whirlpool in appliances revealed significant enhancements in control performance and robustness.

The paper is organized as follows: Section II covers motor and inverter modeling, Section III details the control design including the DTVSC speed controller and FCS-MPC current controller, Section IV presents simulation results, and Section V summarizes the findings.

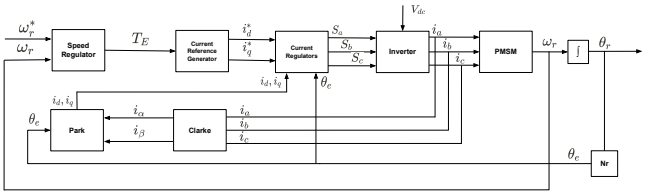

Fig. 1: Block scheme of the proposed cascade controller (FOC)

II. Background

A. PMSM Model

The PMSM electrical model in the (d, q) reference frame is given by:

$$\begin{cases} \dfrac{di_d(t)}{dt} = & -\dfrac{Ri_d(t)}{L} + \omega_e(t)i_q(t) + \dfrac{u_d(t)}{L} + d_d(t) \\ \dfrac{di_q(t)}{dt} = & -\dfrac{Ri_q(t)}{L} - \omega_e(t)\left[i_d(t) + \dfrac{\lambda_0}{L}\right] + \dfrac{u_q(t)}{L} \\ & +d_q(t) \end{cases} \quad (1)$$

where $i_d(t)$ and $i_q(t)$ are the $d-axis$ and $q-axis$ stator currents, respectively, and $u_d(t)$ and $u_q(t)$ are the corresponding voltages; R is the winding resistance, L is the winding inductance on axis d and q and λ_0 is the flux linkage of the permanent magnet; $\omega_e(t)$ is the electrical angular motor speed, while $d_d(t)$ and $d_q(t)$ represent the overall uncertainties (parameter variations and disturbances). The motor electrical torque $T_E(t)$ is:

$$T_E(t) = K_t i_q(t) \quad (2)$$

while $P(t)$, the mechanical power, is $P(t) = T_E(t)\omega_r(t)$. In (2), $K_t = \dfrac{3}{2}\lambda_0 N_r$ is the torque constant, being N_r the number of pole pairs, and $\omega_r(t)$ is the mechanical angular motor speed. The torque $T_E(t)$ is proportional to $i_q(t)$ because of the assumption that there is no reluctance torque in the considered PMSM [13].

The motor mechanics are described by:

$$\begin{cases} \dfrac{d\theta_r(t)}{dt} = & \omega_r(t) \\ \dfrac{d\omega_r(t)}{dt} = & -\dfrac{B\omega_r(t)}{J} + \dfrac{T_E(t) - T_L(t)}{J} + d_r(t) \end{cases} \quad (3)$$

where $\theta_r(t)$ denotes the motor mechanical angular position, J is the motor plus load inertia moment, B is the viscous friction coefficient, $T_L(t)$ is the unknown load torque, and $d_r(t)$ represents the remaining uncertainties (parameter variations and general disturbances different from $T_L(t)$).

The electrical and mechanical quantities are related by N_r:

$$\omega_e(t) = N_r\omega_r(t); \qquad \theta_e(t) = N_r\theta_r(t). \quad (4)$$

Finally, the following assumption is made:

Assumption 2.1: The uncertainty terms $d_d(t)$, $d_q(t)$, $T_L(t)$ and $d_r(t)$ are bounded:

$$|d_d(t)| \leq \rho_d; \quad |d_q(t)| \leq \rho_q; \quad J\,|d_r(t)| + |T_L(t)| \leq \rho_r. \quad (5)$$

being ρ_d, ρ_q, ρ_r known constants.

Defining Δt as the sampling time, $t_i = i \cdot \Delta t$, being $i = 0, 1 \ldots$, and considering Eulero approximation, electrical and mechanical models (1), (3) can be discretized as follows:

$$\begin{bmatrix} i_d(t_{i+1}) \\ i_q(t_{i+1}) \end{bmatrix} = [I + \Delta t A_m(t_i)] \begin{bmatrix} i_d(t_i) \\ i_q(t_i) \end{bmatrix} - \begin{bmatrix} 0 \\ \dfrac{\omega_e(t_i)\lambda_0 \Delta t}{L} \end{bmatrix} + \Delta t \left\{ B_m \begin{bmatrix} u_d(t_i) \\ u_q(t_i) \end{bmatrix} + \begin{bmatrix} d_d(t_i) \\ d_q(t_i) \end{bmatrix} \right\} \quad (6)$$

where:

$$A_m(t_i) = \begin{bmatrix} -\dfrac{R}{L} & \omega_e(t_i) \\ -\omega_e(t_i) & -\dfrac{R}{L} \end{bmatrix}; \quad B_m = \begin{bmatrix} \frac{1}{L} & 0 \\ 0 & \frac{1}{L} \end{bmatrix}.$$

$$\begin{cases} \theta_r(t_{i+1}) = & \theta_r(t_i) + \Delta t \cdot \omega_r(t_i) \\ \omega_r(t_{i+1}) = & \omega_r(t_i) + \Delta t \left[\dfrac{-B\omega_r(t_i) + T_E(t_i) - T_L(t_i)}{J} \right] \\ & +\Delta t \cdot d_r(t_i) \end{cases} \quad (7)$$

B. Inverter Model

As illustrated in Fig. 2, an inverter primarily consists of six switches, positioned in the upper and lower legs of the circuit. In each leg of an inverter, only one switch can be turned on (represented as "1") while the other remains off (represented as "0") at any given time to prevent a short circuit. As a result, the six switches can be turned on and off in a total of eight different combinations, which can be represented by the state of their upper switches, as shown in Tab. I.

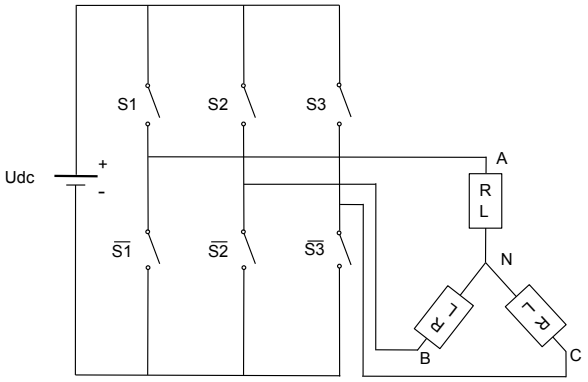

Fig. 2: Inverter structure

TABLE I: Switching states of inverter

	U_0	U_1	U_2	U_3	U_4	U_5	U_6	U_7
S_1	0	1	1	0	0	0	1	1
S_2	0	0	1	1	1	0	0	1
S_3	0	0	0	0	1	1	1	1

The three-phase voltages relative to the neutral point of the PMSM, represented as U_{AN}, U_{BN}, and U_{CN}, correspond to the voltage differences between the inverter output and the neutral point, as depicted in Fig. 2. The conversion of three-phase voltage components into the $\alpha - \beta$ frame is made using the Clarke transformation. As stated in [3] [4], the $\alpha-\beta$ voltages are expressed in terms of the switching states of the three upper-leg switches (S_1, S_2 and S_3):

$$\begin{bmatrix} u_\alpha \\ u_\beta \end{bmatrix} = \frac{2}{3} U_{dc} \begin{bmatrix} 1 & -\frac{1}{2} & -\frac{1}{2} \\ 0 & \frac{\sqrt{3}}{2} & -\frac{\sqrt{3}}{2} \end{bmatrix} \begin{bmatrix} S_1 \\ S_2 \\ S_3 \end{bmatrix} \tag{8}$$

where U_{dc} represents the DC power supply. The $d-q$ axis voltages are obtained by applying the Park transformation to the stationary frame $\alpha - \beta$ voltages [3], [4]:

$$\begin{bmatrix} u_d \\ u_q \end{bmatrix} = \begin{bmatrix} \cos\theta_e & \sin\theta_e \\ -\sin\theta_e & \cos\theta_e \end{bmatrix} \begin{bmatrix} u_\alpha \\ u_\beta \end{bmatrix} \tag{9}$$

By replacing (8) into (9), it follows that for a given electrical angle θ_e, only eight specific pairs of u_d and u_q values can be precisely achieved by the VSI inverter. These correspond to the switching states (S_1, S_2 and S_3) listed in Table I. These constraints limit the control actions to a finite control set of parameters [3], [4].

III. CONTROL DESIGN

A. FOC Structure

FOC is a widely used methodology for managing stator currents through vector control in the *d-q* coordinate system. At its core, FOC employs a state transformation technique to decouple the dynamics of torque and flux, enabling more precise and independent control of these two critical aspects. This decoupling is achieved within the rotating $d-q$ reference frame, as illustrated in Fig. 1 [1]. The control system is organized into two primary loops. The inner loop is responsible for current regulation, ensuring that $i_d(t)$, the direct-axis current, is maintained at zero. This condition represents typical motor operation under standard speed ranges and excludes scenarios such as field weakening [23]. By maintaining $i_d(t) = 0$ the flux remains constant, simplifying the torque control. The outer loop, in turn, manages the angular speed of the motor, by indirectly controlling the electrical torque $T_E(t)$, which serves as the system main control variable. Since $T_E(t)$ depends on the quadrature-axis current $i_q(t)$ as per equation (2), the controller cannot directly assign its value. Instead, it computes the desired torque ${T_E}^*(t)$ and translates it into a target current ${i_q}^*(t)$ using the relation ${T_E}^*(t) = K_t {i_q}^*(t)$. The current $i_q(t)$ is then regulated to track ${i_q}^*(t)$, ensuring the motor delivers the required torque. This two-loop structure, with the inner loop stabilizing current and the outer loop handling speed, provides precise and robust control over motor performance while adhering to FOC principles.

B. Discrete-Time Variable Structure Velocity Control

Let ${\omega_r}^*(t)$ be the reference variable for the mechanical angular speed, and define the tracking error $e_\omega(t)$ as $e_\omega(t) = \omega_r(t) - {\omega_r}^*(t)$. Defining $s_\omega(t)$ as:

$$s_\omega(t) = e_\omega(t) + \lambda_\omega \int_0^t e_\omega(\tau) d\tau \tag{10}$$

with $\lambda_\omega > 0$, the sliding surface $s_\omega(t) = 0$ guarantees the asymptotic zeroing of $e_\omega(t)$. Using Eulero approximation, the sampled variable $s_\omega(t_{i+1})$ can be introduced:

$$s_\omega(t_{i+1}) = s_\omega(t_i) + e_\omega(t_{i+1}) - (1 - \lambda_\omega \cdot \Delta t)\, e_\omega(t_i) \tag{11}$$

Adding and subtracting the quantity $\lambda_2 s_\omega(t_i)$ in (11), with $0 < \lambda_2 < 1$, and defining $\sigma(t_{i+1}) \triangleq s_\omega(t_{i+1}) - \alpha_2 s_\omega(t_i)$, with $\alpha_2 = 1 - \lambda_2$, expression (11) can be written as:

$$\sigma(t_{i+1}) = e_\omega(t_{i+1}) - (1 - \lambda_\omega \cdot \Delta t)\, e_\omega(t_i) + \lambda_2 s_\omega(t_i) \tag{12}$$

Remark 3.1: Since $0 < \alpha_2 < 1$, imposing $\sigma(t_{i+1}) = 0$ ensures the vanishing of $s_\omega(t_i)$ (and, as a consequence, of $e_\omega(t_i)$). At the same time, the introduction of the "tuning knob" α_2 allows to improve the transient shaping of the system response.

Theorem 3.1: Consider system (7) and $\sigma(t_{i+1})$ given by (12). The following control law:

$$T_E(t_i) = T_E^{(eq)}(t_i) + T_E^{(n)}(t_i) \tag{13}$$

with:

$$T_E^{(eq)}(t_i) = B\omega_r(t_i) - J\left[\lambda_\omega e_\omega(t_i) + \frac{\lambda_2}{\Delta t} s_\omega(t_i)\right] \tag{14}$$

$$T_E^{(n)}(t_i) = \begin{cases} \alpha_r \dfrac{J}{\Delta t}\left[|\sigma(t_i)| - \rho_r \Delta t\right] & if \quad |\sigma(t_i)| > \rho_r \Delta t \\ 0 & if \quad |\sigma(t_i)| \le \rho_r \Delta t \end{cases} \tag{15}$$

and $|\alpha_r| < 1$, guarantees a quasi sliding mode [21] on $\sigma(t_{i+1}) = 0$, i.e. the vanishing of the tracking error $e_\omega(t_i)$.

Proof: Assuming that $\omega_r^*(t_{i+1}) \simeq \omega_r^*(t_i)$, i.e. the reference ${\omega_r}^*(t)$ slowly varies with respect to the sampling time Δt, and using (7), expression (12) becomes:

$$\begin{aligned} \sigma(t_{i+1}) = \frac{\Delta t}{J} \{ & -B\omega_r(t_i) + T_E(t_i) - T_L(t_i) \\ & + J\left[d_r(t_i) + \lambda_\omega e_\omega(t_i) + \frac{\lambda_2}{\Delta t} s_\omega(t_i)\right]\Big\} \end{aligned} \tag{16}$$

Replacing (13) and (14) in (16), one has:

$$\sigma(t_{i+1}) = \frac{\Delta t}{J}\left[-T_L(t_i) + J d_r(t_i) + T_E^{(n)}(t_i)\right] \tag{17}$$

Finally, the quasi sliding mode existence condition [21]:

$$|\sigma(t_{i+1})| < |\sigma(t_i)| \tag{18}$$

is fulfilled by (29). ■

C. FCS Predictive Current Control

After the control signal trajectories in the d–q reference frame are defined based on the electrical angle θ_e (as given in Equation 9), and assuming that PWM is not used in generating the control signals, the possible choices for u_d and u_q are restricted to the eight alternatives described in Subsection II-B. These eight combinations of u_d and u_q corresponding to a particular sampling instant and electrical angle θ_e, form the candidate set for the FCS. To determine which pair should be applied at the sampling time t_i, an objective function is used, defined as follows [3] [4]:

$$J = \begin{bmatrix} i_d^*(t_i) - i_d(t_{i+1}) & i_q^*(t_i) - i_q(t_{i+1}) \end{bmatrix} \begin{bmatrix} i_d^*(t_i) - i_d(t_{i+1}) \\ i_q^*(t_i) - i_q(t_{i+1}) \end{bmatrix} \tag{19}$$

By replacing (6) in (19), considering all the disturbances equal to zero, the objective function J will include the currents measured at the sampling time t_i and the manipulated variables u_d and u_d, as follows:

$$\begin{aligned} J = & [i_d^*(t_i) - i_d(t_i) - \frac{\Delta t}{L}(u_d(t_i) - Ri_d(t_i) + \omega_e(t_i)Li_q(t_i))]^2 \\ & + [i_q^*(t_i) - i_q(t_i) - \frac{\Delta t}{L}(u_q(t_i) - Ri_q(t_i) - \omega_e(t_i)Li_d(t_i) \\ & - \omega_e(t_i)\lambda_0)].^2 \end{aligned} \tag{20}$$

In the following step, the objective function J is evaluated for each of the eight candidate pairs $u_d(t_i)$ and $u_q(t_i)$, yielding a set of values J_0, J_1, J_2, ... , J_7. A straightforward search algorithm is then used to find the minimum among these values and identify its corresponding index. This index is then used to determine the appropriate control signal for the VSI at time t_i, based on Table I. The core principle of the finite control set approach lies in the concept of receding horizon control, which involves making one-step-ahead predictions and performing real-time optimization to solve the constrained optimal control problem. As a result, the associated algorithm is referred to as the FCS-MPC algorithm.

D. FCS-MPC System Analysis

As reported in [3], [24], for analyzing the FCS predictive control algorithm, the following definition is introduced:

$$\begin{bmatrix} f_d(t_i) \\ f_q(t_i) \end{bmatrix} := \begin{bmatrix} i_d^*(t_i) \\ i_q^*(t_i) \end{bmatrix} \quad -(I + \Delta t A_m(t_i)) \begin{bmatrix} i_d(t_i) \\ i_q(t_i) \end{bmatrix} + \begin{bmatrix} 0 \\ \frac{\omega_e(t_i)\lambda_0 \Delta t}{L_q} \end{bmatrix} \tag{21}$$

By combining (21) and (6), it can be shown [3] [24] that (19) assumes the following form:

$$\begin{aligned} J \quad = \quad & \left(\begin{bmatrix} u_d(t_i) \\ u_q(t_i) \end{bmatrix} - (\Delta t^2 B_m^T B_m)^{-1} B_m^T \Delta t \begin{bmatrix} f_d(t_i) \\ f_q(t_i) \end{bmatrix} \right)^T \\ \times \quad & (\Delta t^2 B_m^T B_m) \\ \times \quad & \left(\begin{bmatrix} u_d(t_i) \\ u_q(t_i) \end{bmatrix} - (\Delta t^2 B_m^T B_m)^{-1} B_m^T \Delta t \begin{bmatrix} f_d(t_i) \\ f_q(t_i) \end{bmatrix} \right) \end{aligned} \tag{22}$$

Function J has a minimum value of zero when the optimal control variables $u_d(t_i)$ and $u_q(t_i)$ are selected as follows:

$$\begin{aligned} \begin{bmatrix} u_d^{\text{opt}}(t_i) \\ u_q^{\text{opt}}(t_i) \end{bmatrix} &= (\Delta t^2 B_m^T B_m)^{-1} \Delta t B_m^T \begin{bmatrix} f_d(t_i) \\ f_q(t_i) \end{bmatrix} \\ &= \frac{1}{\Delta t} \begin{bmatrix} L & 0 \\ 0 & L \end{bmatrix} \begin{bmatrix} f_d(t_i) \\ f_q(t_i) \end{bmatrix}. \end{aligned} \tag{23}$$

This is the optimal solution using a one-step-ahead prediction. Replacing (23) into (22), the objective function can be also expressed as:

$$J = \frac{\Delta t^2}{L^2} \left\{ \left[u_d(t_i) - u_d^{\text{opt}}(t_i) \right]^2 + \left[u_q(t_i) - u_q^{\text{opt}}(t_i) \right]^2 \right\} \tag{24}$$

Since optimal control signals (23) do not take into account the uncertainties present in model (6), in the next section they will be replaced with a control law derived using DTVSC, in order to improve system robustness.

E. Variable Structure based FCS Predictive Current Control

As discussed in Subsection III-D and developed in [3], [24], the main feature of the finite control set scheme is an optimal output feedback control employing (23).

Following the description given in Section III-A, the electrical torque $T_E(t_i)$ cannot be assigned directly by the outer loop controller. Instead, the computed $T_E(t_i)$ in (13) represents the desired torque $T_E^*(t_i)$, which needs to be translated into a target current $i_q^*(t_i)$ using the relation $i_q^*(t_i) = \frac{T_E^*(t_i)}{K_t}$. The current $i_q(t_i)$ is then regulated to track $i_q^*(t_i)$, ensuring the motor delivers the required torque. At the same time, the current $i_d(t_i)$ needs to be regulated to zero. The control of both the currents $i_q(t_i)$, $i_d(t_i)$ is ensured by the following Theorem.

Theorem 3.2: Consider system (6), define the error $e_q(t_i) = i_q(t_i) - i_q^*(t_i)$ and the discrete time sliding surfaces:

$$s_d(t_i) = i_d(t_i) - \lambda_d i_d(t_{i-1}) = 0 \tag{25}$$

$$s_q(t_i) = e_q(t_i) - \lambda_q e_q(t_{i-1}) = 0 \tag{26}$$

The following control laws:

$$u_d(t_i) = u_d^{(eq)}(t_i) + u_d^{(n)}(t_i); \quad u_q(t_i) = u_q^{(eq)}(t_i) + u_q^{(n)}(t_i) \tag{27}$$

with:

$$u_d^{(eq)}(t_i) = Ri_d(t_i) - L\omega_e(t_i)i_q(t_i) - \frac{L}{\Delta t}(1 - \lambda_d)i_d(t_i)$$

$$u_d^{(n)}(t_i) = \begin{cases} \alpha_d \frac{L}{\Delta t} \left[|s_d(t_i)| - \rho_d \Delta t \right] & if \quad |s_d(t_i)| > \rho_d \Delta t \\ 0 & if \quad |s_d(t_i)| \leq \rho_d \Delta t \end{cases} \tag{28}$$

$$u_q^{(eq)}(t_i) = Ri_q(t_i) + \omega_e(t_i)\left[Li_d(t_i) + \lambda_0\right] - \frac{L}{\Delta t}(1-\lambda_q)e_q(t_i)$$

$$u_d^{(n)}(t_i) = \begin{cases} \alpha_q \dfrac{L}{\Delta t}\left[|s_q(t_i)| - \rho_q \Delta t\right] & if \quad |s_q(t_i)| > \rho_q \Delta t \\ 0 & if \quad |s_q(t_i)| \leq \rho_q \Delta t \end{cases} \tag{29}$$

and $|\alpha_d| < 1$, $|\alpha_q| < 1$, achieve a quasi sliding mode [21] on (25), (26), i.e. the zeroing of $i_d(t_i)$ and $e_q(t_i)$.

Proof: The proof is omitted for the sake of brevity ■

IV. SIMULATION RESULTS

In order to verify the validity of the proposed approach, the highly accurate Whirlpool program for simulating household appliance has been used. Numerical simulations were conducted on the model of a PMSM drain pump mounted in a Whirlpool dishwasher. The nominal parameters of the PMSM are listed in Table II. The simulations are also aimed at comparing the performances of the proposed approach with a PI control, currently implemented on several Whirlpool productions, while tracking the speed profile shown in Fig.3. In order to assess how the selection of the sampling rate influences the closed-loop performance, two different sampling intervals were employed in the simulation experiments: $\Delta t = 1 \times 10^{-5} s$ and $\Delta t = 1 \times 10^{-6} s$. The external speed control loop is set to compute at a lower sampling rate with a sampling interval of $\Delta t = 1 \times 10^{-4} s$. The chosen parameters for both controllers are listed in Table III. Figure 4 shows the behavior of the controlled variable over a specific time interval, from time instant $7.8s$ to time instant $8.8s$. Indeed, it is in this interval that a sudden variation of the load torque occur, simulating the scenario where the pump is drained out, and the motor impeller works in the air. In this instance, the sensitivity of the PI speed control to the torque drop is evident, leading to a large overshoot in the speed signal. On the contrary, the proposed control returns a smaller deviation from the reference and a faster recovery after the peak. The corresponding electrical torques are shown in Fig.5-6. It can easily be seen that by increasing the sampling frequency, the control of electrical torque is greatly improved producing a controlled signal with less pronounced oscillations. Therefore, it is evident how he selection of Δt is crucial in the design and implementation of the FCS method. Overall, the proposed control exhibited a greater promptness and accuracy if compared to the PI control. To quantify the quality of the control action, two indices were evaluated: the Integral Absolute Error (IAE) and the Mean Squared Error (MSE). As showed in Table IV, the index values for the proposed control are lower than those for the PI control, pointing out the higher performance achieved by the investigated solution.

TABLE II: PMSM parameters

Coil dependent parameters		
Phase-phase resistance	ohm	45.5
Phase-phase inductance	mH	120
Flux linkage	Vpk/rad/s	0.0857
Torque constant	Nm/A	0.12855
Pole pairs	–	1
Dynamic parameters		
Max. current	A peak	0.6
Max. torque	Nm	0.07
Max. speed	rpm	4000
Mechanical parameters		
Rotor inertia	$\text{Kgm}^2 \cdot 10^{-6}$	2.13
Friction Coefficient	Nm/ rad/s $\cdot 10^{-5}$	7.40

TABLE III: Control scheme parameters

DTVSC (Speed Regulator)	**PI (Speed Regulator)**
$\lambda_\omega = 600$ $\lambda_2 = 0.6$ $\alpha_r = 0.01$ $\rho_r = 300$ $\Delta t = 1 \times 10^{-4}$	$K_p = 8.40e-05$ Nm/(rad/s) $K_i = 1.47e-03$ Nm/(rad)
DTVSC (Currents Regulators)	**PI (Currents Regulators)**
$\lambda_d = 0.1 \quad \lambda_q = 0.1$ $\alpha_d = 0.95 \quad \alpha_q = 0.99$ $\rho_d = 0.5 \quad \rho_q = 0.5$ $\Delta t = 1 \times 10^{-5}/1 \times 10^{-6}$ s	$K_p = 237.0$ V/A $K_i = 221079$ V/(A*s)

TABLE IV: Experimental Results: Performance Indeces

Performance Indeces	IAE	MSE
PI controller	423.9704	$9.5881e^{+03}$
Proposed controller	0.1416	0.0056

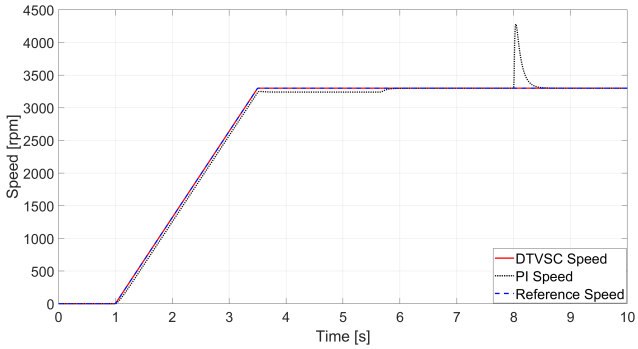

Fig. 3: Mechanical speed: reference (dashed blue line), PI controller (black dotted line), DTVSC controller (red continuous line).

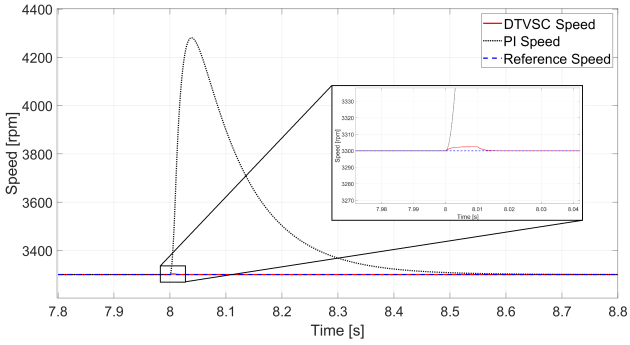

Fig. 4: Mechanical Speed: load torque variation

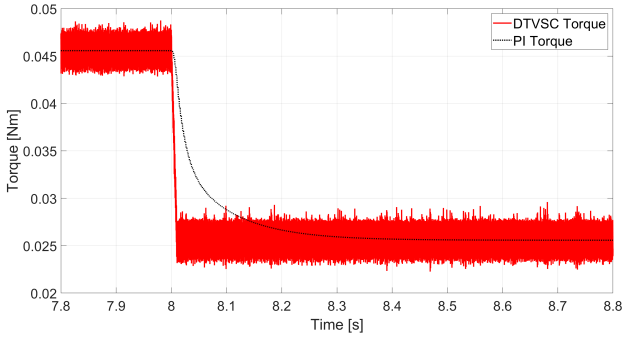

Fig. 5: Electrical Torque (Sample time $\Delta t = 1 \times 10^{-5} s$)

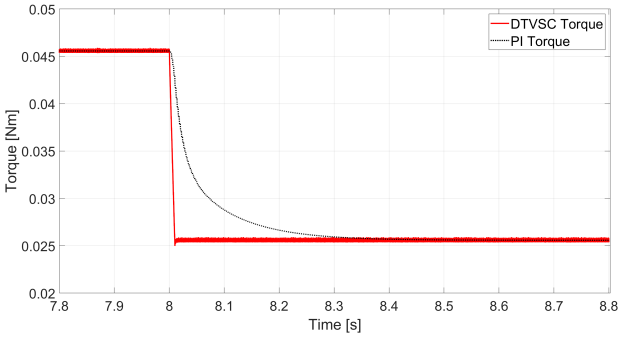

Fig. 6: Electrical Torque (Sample time $\Delta t = 1 \times 10^{-6} s$)

V. CONCLUSIONS

Utilizing the highly accurate Whirlpool household appliance numerical simulator, this paper demonstrates that the proposed DTVSC velocity regulator, paired with FCS-MPC current control for PMSMs, achieves superior speed trajectory tracking and robustness compared to traditional PI-based FOC.

REFERENCES

[1] P. Vas, *Vector control of AC machines*. London, U.K.: Oxford Univ. Press, 1990.

[2] G. Buja and M. Kazmierkowski, "Direct torque control of PWM inverter-fed AC motors - a survey," *IEEE Transactions on Industrial Electronics*, vol. 51, no. 4, pp. 744–757, 2004.

[3] L. Wang, S. Chai, D. Yoo, L. Gan, and K. Ng, *PID Control System Design for Electrical Drives and Power Converters*. Wiley-IEEE Press, 2015.

[4] S. Chai and L. Wang, "Finite control set model predictive control of 2LVSI-PMSM using interpolated switching states," in *IECON 2012 - 38th Annual Conference on IEEE Industrial Electronics Society*, 2012, pp. 1799–1804.

[5] S. Kouro, P. Cortes, R. Vargas, U. Ammann, and J. Rodriguez, "Model predictive control? A simple and powerful method to control power converters," *IEEE Transactions on Industrial Electronics*, vol. 56, no. 6, pp. 1826–1838, 2009.

[6] F. Morel, X. Lin-Shi, J.-M. Retif, B. Allard, and C. Buttay, "A comparative study of predictive current control schemes for a permanent-magnet synchronous machine drive," *IEEE Transactions on Industrial Electronics*, vol. 56, no. 7, pp. 2715–2728, 2009.

[7] V. Ambrozic, D. Nedeljkovic, and R. Fiser, "New current regulation principle [for power convertors]," in *IEMDC 2001. IEEE International Electric Machines and Drives Conference (Cat. No.01EX485)*, 2001, pp. 979–984.

[8] P. Cortes, M. P. Kazmierkowski, R. M. Kennel, D. E. Quevedo, and J. Rodriguez, "Predictive control in power electronics and drives," *IEEE Transactions on Industrial Electronics*, vol. 55, no. 12, pp. 4312–4324, 2008.

[9] S. Kouro, M. A. Perez, J. Rodriguez, A. M. Llor, and H. A. Young, "Model predictive control: MPC's role in the evolution of power electronics," *IEEE Industrial Electronics Magazine*, vol. 9, no. 4, pp. 8–21, 2015.

[10] C. S. Lim, E. Levi, M. Jones, N. A. Rahim, and W. P. Hew, "FCS-MPC-based current control of a five-phase induction motor and its comparison with PI-PWM control," *IEEE Transactions on Industrial Electronics*, vol. 61, no. 1, pp. 149–163, 2014.

[11] X. Liu, H. Yang, S. Cai, H. Lin, F. Yu, and Y. Yang, "A novel finite-control-set model-free predictive current control incorporating event triggering mechanism for PMSM drives," *IEEE Transactions on Industry Applications*, vol. 61, no. 1, pp. 322–334, 2025.

[12] A. Pisano, A. Davila, L. Fridman, and E. Usai, "Cascade control of PM DC drives via second-order sliding-mode technique," *IEEE Trans. Ind. Electron.*, vol. 55, no. 11, pp. 3846–3854, 2008.

[13] V. I. Utkin, J. Guldner, and J. Shi, *Sliding mode control in electromechanical systems*, ser. Systems and Control. Florida, USA: CRC Press LLC, 1999.

[14] A. Sabanovic, K. Jezernik, and N. Sabanovic, "Sliding modes applications in power electronics and electrical drives," in *Variable Structure Systems: Towards the 21st Century*, X. Yu and J.-X. Xu, Eds. Berlin,Germany: Springer-Verlag, 2002, vol. 274, pp. 223–251.

[15] T. L. Chern and J. S. Wong, "DSP based integral variable structure control for DC motor servo drives," *Proc. Inst. Elect. Eng. Control Theory Appl.*, vol. 142, no. 5, pp. 444–450, 1995.

[16] C. Attaianese, A. Perfetto, and G. Tomasso, "Robust position control of DC drives by means of controllers," *Proc. Inst. Elect. Eng..Elect. Power Appl.*, vol. 146, no. 4, pp. 391–396, 1999.

[17] H. Butler, G. Honderd, and J. van Amerongen, "Model reference adaptive control of a direct-drive DC motor," *IEEE Control Syst. Mag.*, vol. 9, no. 1, pp. 80–84, 1989.

[18] P. Dobra, "Robust PI control for servo DC motors," in *Proc. IEEE Int. Conf. Control Appl.*, 2002, pp. 100–101.

[19] K. Ohishi, M. Nakao, K. Ohnishi, and K. Miyachi, "Microprocessor-controlled DC motor for load-insensitive position servo system," *IEEE Trans. Ind. Electron.*, vol. IE-34, no. 1, pp. 44–49, 1987.

[20] J. O. Jang, "Neural network saturation compensation for DC motor systems," *IEEE Trans. Ind. Electron.*, vol. 54, no. 3, pp. 1763–1767, 2007.

[21] K. Furuta, "Vss type self-tuning control," *IEEE Trans. Ind. Electron.*, vol. 40, no. 1, pp. 37–44, 1993.

[22] O. Kaynak and A. Denker, "Discrete-time sliding mode control in the presence of system uncertainty," *Int. J. Contr.*, vol. 57, no. 5, p. 1177–1189, 1993.

[23] J. Shi and Y. Lu, "Field-weakening operation of cylindrical permanent-magnet motors," in *Proc. IEEE Int. Conf. on Contr. Appl.*, Dearborn, MI, sep. 1996, pp. 864–869.

[24] L. Wang and L. Gan, "Integral FCS predictive current control of induction motor drive," *IFAC Proceedings Volumes*, vol. 47, no. 3, pp. 11 956–11 961, 2014, 19th IFAC World Congress.